Finite Element Model of a Bilayered Gold-Coated Carbon Nanotube Composite Surface

Hong Liu, John W. McBride, *Senior Member, IEEE*, Michael Peter Down, and Suan Hui Pu, *Member, IEEE*

***Abstract*— Vertically aligned multiwalled carbon nanotubes (MWCNTs), with a gold (Au)-coated surface, have been shown to provide a stable contact resistance for electrical contact switching applications under low force conditions (micronewton to millinewton), with the MWCNT surface providing a compliant support for the conducting Au layer. In this paper, nanoindentation results are used in the development of a finite element contact model for the composite, referred to as Au/CNT. The results show that the surface is best modeled as a bilayered structure, in which the top layer is modeled as an elastic–plastic layer of the Au/CNT mixed material and the under layer as a CNT forest. The resultant model matches the experimental results for a range of samples with different thickness configurations.**

***Index Terms*— Bilayered, carbon nanotubes (CNTs), contact mechanics, finite element (FE) modeling.**

I. Introduction

FOR MEMS microswitches, a stable and low contact resistance is required, typically $<1\ \Omega$. Commonly used materials for ohmic microswitches include gold, palladium, platinum [1], ruthenium [2], rhodium [3], and gold alloy [4]; but the weakness of such materials is that they are relatively soft and therefore wear easily. Other materials like silicon carbide and diamond films have low electrical conductivity and are unsuitable for electrical contact application [5]. The application of Au-coated multiwalled carbon nanotubes (MWCNTs) as contact surfaces was first investigated in [6], where the forest of CNT is used to create a compliant under layer to a metallic film. Early studies [7]–[10] showed that a CNT-coated surface had potential as a contact material for MEMS switches. It was also noted that the compliant surface described could be used for thermal applications.

Manuscript received October 26, 2014; accepted April 8, 2015. This work was supported in part by the Ministry of High Education, Malaysia, under Grant FRGS-12014-TK01-USMC-1 and in part by the Innovative Electronics Manufacturing Research Centre through the Engineering and Physical Sciences Research Council under Grant EP/H03014X/1. Recommended for publication by Associate Editor T. J. Schoepf upon evaluation of reviewers' comments.

H. Liu and S. H. Pu are with the University of Southampton–Malaysia Campus, Johor Bahru 79200, Malaysia (e-mail: hl1v13@soton.ac.uk; suanhui.pu@southampton.ac.uk).

J. W. McBride is with the University of Southampton–Malaysia Campus, Johor Bahru 79200, Malaysia, and also with the Faculty of Engineering and the Environment, University of Southampton, Southampton SO17 1BJ, U.K. (e-mail: j.w.mcbride@soton.ac.uk).

M. P. Down is with the Faculty of Engineering and the Environment, University of Southampton, Southampton SO17 1BJ, U.K. (e-mail: mpd2g12@soton.ac.uk).

Color versions of one or more of the figures in this paper are available online at http://ieeexplore.ieee.org.

Digital Object Identifier 10.1109/TCPMT.2015.2428612

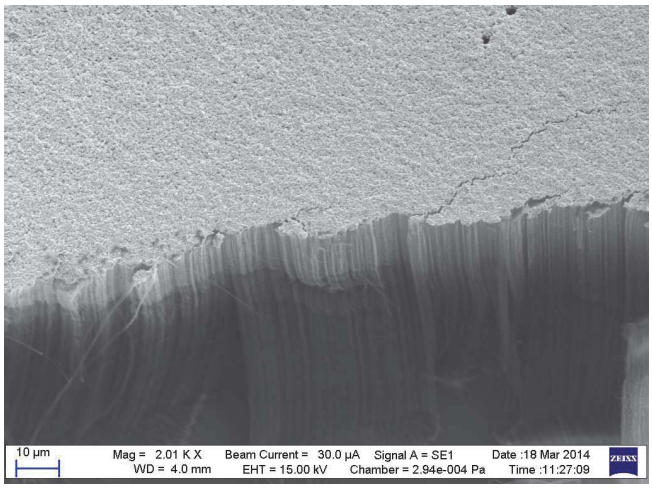

Fig. 1. Sample of nominal 500-nm gold coated on 50-μm CNT.

Individual CNTs show a very high elastic modulus [11]–[13], but when grown as a vertical aligned forest, they form a compliant surface with the effective modulus reduced by several orders of magnitude [14]. Bending, buckling [15], and the waviness of individual CNT [14] are proposed as the main mechanisms for the reduction of the elastic modulus.

The nanoindentation technique has been used to measure the mechanical properties and the effective modulus of vertically aligned CNT films [14], [16]. However, a gold-coated CNT (Au/CNT) surface presents a more complex surface. Scanning electron microscope (SEM) images show that a gold layer of nominally 500-nm thickness does not form a continuous film, but penetrates into the CNT forest, as shown in Fig. 1. Initial nanoindentation studies of the Au/CNT composite [18], [19] showed that the depth of the Au penetrated had a large effect on the mechanical properties. In [19], an initial bilayered contact model was developed, where the top layer was modeled as an elastic–plastic composite and under layer as CNT forest. The simulation results matched well with the experimental results for samples with 30-μm height CNT. In this paper, the simulations results are extended for samples with different height (thickness) configurations. The aim is to develop a robust finite element (FE) model to describe the Au/CNT composite and to allow the optimization of the surface for an MEMS switching application where a stable contact resistance is the primary design requirement.

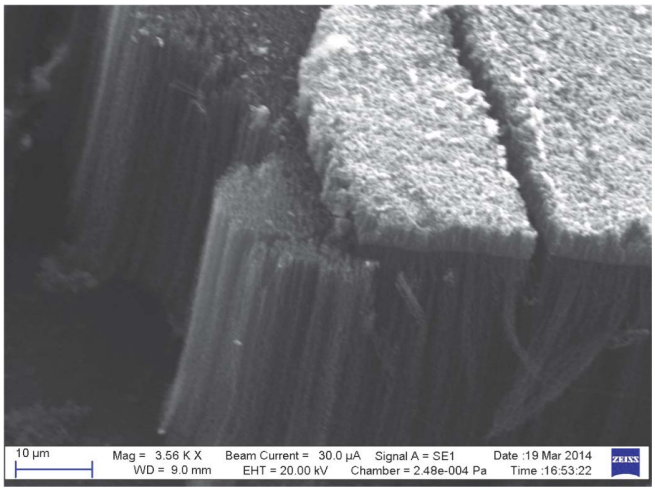

Fig. 2. Sample of nominal 300-nm gold coated on 30-μm CNT: 4–5 μm of Au penetrates into MWCNT.

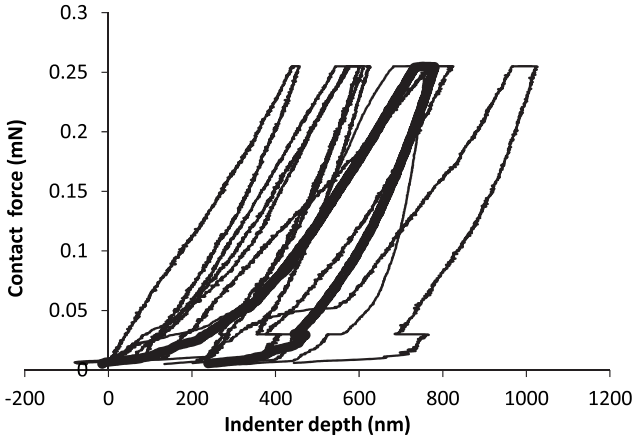

Fig. 3. Nanoindentation results for the composite 500-nm gold coated on 50-μm CNT, under 0.25 mN. The thin lines are the experimental results, and the thick line is the averaged curve.

II. Sample Preparation and Nanoindentation Test Setup

The production of the Au/CNT composite is detailed in [18]. Three heights (thickness) of CNT forest were grown, 30, 50, and 80 μm. Three nominal thicknesses of sputtered Au were used, 300, 500, and 800 nm, to generate a matrix of nine different layer configurations. The nominal Au thickness is measured on a sectioned sample of Au sputtered on to a Si wafer, measured using a laser profiler. The thickness of the Au coating on the CNT does not conform to the nominal value. Fig. 1 shows a nominal 500-nm coating, where the sectioned surface is in the center of the CNT forest. Fig. 2 shows a nominal 300-nm coating section where the Au upper layer has separated as a result of the disruptive sectioning. The roughness (Ra) is approximately 1.3 μm with 500-nm Au coated on 30-μm CNT [8].

Nanoindentation tests were undertaken using a Micro-Materials Nanotest Vantage. Since the standard Berkovich tip would pierce the gold film and separate the CNT [18], the test were performed with a 200-μm radius diamond indenter tip.

Each sample was subjected to four loads, 0.25, 0.5, 0.75, and 1 mN, with each load cycle repeated 10 times, at a new location on the surface. Some of the samples failed at 1 mN and as a consequence are not used in this paper.

During nanoindentation test, the loading and unloading rate was set as 0.01 mN/s. Vertical aligned CNTs are known to show viscoelastic behavior [20], which will result in creep deformation. To minimize the effect of creep, the peak load was held for 30 s before unloading started, as shown in Fig. 3, where the creep deformation for the composite 500-nm Au/50-μm CNT at 0.25 mN is about 60 nm.

The elastic modulus and hardness are calculated automatically using the Oliver and Pharr model [21], [22] after creep has occurred. Hardness is calculated by classical theory, as in

$$H = P_{\max}/A \tag{1}$$

where H is the hardness and $P_{\max}$ is the maximum load. A is the projected contact area, and can be expressed as a function of contact depth h_c, as $A(h_c)$. In this paper, A is calculated with area function as described in [23], where no roughness is included.

The effective elastic modulus E_r is evaluated and the elastic modulus of specimen E can be then calculated by the following equations:

$$E_r = \frac{\sqrt{\pi}}{2\beta}\frac{S}{\sqrt{A(h_c)}} \tag{2}$$

$$\frac{1}{E_r} = \frac{1-\nu_i^2}{E_i} + \frac{1-\nu^2}{E} \tag{3}$$

where β is a constant depending on the geometry of the indenter, S is the slope of the curve during the initial stages of unloading, also named contact stiffness, E and ν are Young's modulus and Poisson's ratio for the specimen, and E_i and ν_i are the values for the indenter.

Fig. 3 shows the repeated force-depth curves for 50-μm CNT coated with a nominal 500-nm Au, for an applied load of 0.25 mN. The data show the penetration to be variable from 400 to 1000 nm reflecting the irregular nature of the CNT growth and the Au coating. The value of unloading slope S appears to be more repeatable. The properties are calculated based on the averaged curve, shown in Fig. 3, with the anomalies removed, and assuming a single continuum material. The evaluated elastic modulus for samples with 50-μm CNT are shown in Fig. 4. The values demonstrate the response in terms of different layer configurations and provide a reference for FE modeling. The data also show that the mechanical behavior of Au/CNT composite vary with the indenter force, which reveals a bilayered structure behavior [24].

III. Finite Element Modeling

A. Material Models for a Au/CNT Composite

In [19], two models were proposed, defined here as Models I and II. In both models, the Au/CNT composite is considered as continuum material despite the specific form of nanotubes and the possible relative motion between individual tubes. It has been validated that a continuum model can

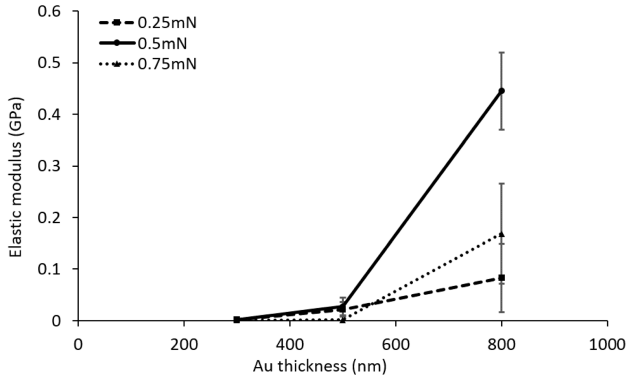

Fig. 4. Elastic modulus from the nanoindentation tests for the composite with different gold nominal thicknesses on 50-μm CNT, and with different load forces.

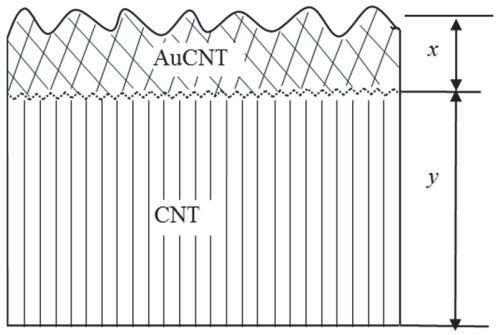

Fig. 5. Illustration of a bilayered model of a Au-coated CNT composite, where x and y are the thickness of the top and under layers, respectively.

be an acceptable simplification for the purpose of modulus predictions [25].

Model I: The Au/CNT composite is a single continuum material. The material properties are from the nanoindentation test. The material is assumed to deform elastic plastically.

Model II: The Au/CNT composite is a bilayered structure, as shown in Fig. 5. As the sputtered gold does not form a uniform layer, but penetrates into the CNT, the top layer is modeled as a mixed material, labeled AuCNT layer herein. The penetration depth is taken as the thickness of the top layer (x). The separation of two layers is represented with a dashed curved line in Fig. 4. Data from the SEM images have been used to estimate the thickness (x) of the AuCNT top layer as follows:

1) 300-nm Au, $x = 4 \pm 1.5$ μm;
2) 500-nm Au, $x = 6 \pm 1.5$ μm;
3) 800-nm Au, $x = 8 \pm 1.5$ μm.

The uncertainty of penetration depth is discussed in Section IV-B.

The under layer is modeled as pure CNT, its thickness is changed according to the nominal thickness of the AuCNT top layer. The default thickness settings for two layers are listed in Table I.

The indentation depth can be from 0.2 to 8 μm, and is usually larger than 20%–30% of the Au penetration depth, so the measured material properties from the nanoindentation tests are the combined effect of AuCNT top layer and CNT under layer [26], and there is no experimental data for material properties of each layer. Based on the indentation tests, approximate values are taken and modified to meet the experimental data, as shown in Table II.

For the AuCNT top layer, the material properties are from the hardest sample (3), the thickest Au and shortest CNT, at low load, i.e., the sample 800-nm Au/30-μm CNT at 0.25 mN. Under this condition, the indenter depth is 148 nm, so that the measurement captured mostly the features of the top layer. For the CNT forest under layer, material properties are from the softest sample (7), thinnest Au, and tallest CNT, at higher load, i.e., 300-nm Au/80-μm CNT at 0.75 mN. The indenter depth can be up to 8 μm, which is the largest depth among the tests, and is assumed to provide the initial estimate for the CNT properties. The material properties for Model II are listed in Table II. The first two rows II(a) are the original setting and the others II(b–d) are the adjusted values, as discussed in Section IV.

Table III lists some of the elastic modulus measured in [14], [16], [20], and [27]. It shows that the elastic modulus of MWCNT forest is generally quite low and variable

TABLE I
DEFAULT THICKNESS SETTING IN FE MODEL II FOR THE TOP AND UNDER LAYERS

Sample number	Composite Au (nm)/CNT(μm)	Top layer x (μm)	Under layer y (μm)
1	300/30	4	26
2	500/30	6	24
(3)	800/30	8	22
4	300/50	4	46
5	500/50	6	44
6	800/50	8	42
(7)	300/80	4	76
8	500/80	6	74
9	800/80	8	72

TABLE II
MATERIAL PROPERTIES IN FE MODELS: MODEL II, CONSIDERING THE COMPOSITE AS A BILAYERED STRUCTURE: AUCNT AS THE TOP LAYER, AND CNT FOREST AS THE UNDER LAYER. THE FIRST TWO ROWS ARE THE ORIGINAL SETTING, AND OTHERS ARE THE ADJUSTED VALUES IN MODELS

Model	Layer	Elastic modulus E (MPa)	Hardness H (MPa)	Poisson's ratio ν
II (a)	Top layer AuCNT	887.455	2.8933	0.21
II (a)	Under layer CNT1	0.726	-	0 [29], [16]
II (b)	Top layer Top1.4	1242.44	4.05	0.21
II (c)	Under layer CNT0.8	0.5808	-	0
II (d)	Under layer CNT7	5.082	-	0
II (e)	Under layer CNT10	7.26	-	0

TABLE III
ELASTIC MODULUS OF VERTICAL ALIGNED MWCNT FOREST

Paper	CNT Thickness (μm)	Elastic modulus E (MPa)	Measured method /Modeling
[20]	10	30	Nanoindenter
[14]	150	0.12-0.27	Nanoindenter based
[16]	98	1.4-2.8	15, 20, 25 μm radius spherical indenter
	150	0.8-2.2	
[27]	100	8	resonator
This work	30	7.26	Modeling: 'CNT10'
	50	5.082	Modeling: 'CNT7'
	80	0.5808	Modeling: 'CNT0.8'

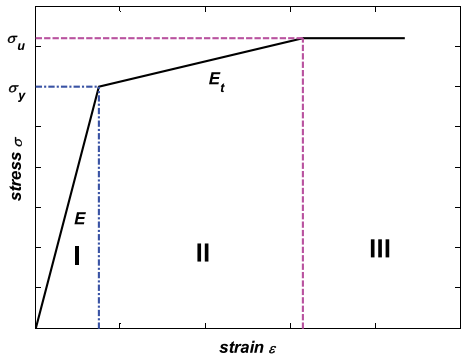

Fig. 6. Stress–strain curves for elastic–plastic material in FE model.

depending on the fabrication process, density and diameter of CNT. Table III also shows that the elastic modulus decreases with the height of CNT [16], [20]. The values used in Model II are also listed at the bottom of Table III.

The top layer AuCNT is modeled as an elastic–plastic material and material option multilinear isotropic hardening (MISO) is defined in ANSYS. Fig. 6 shows a stress–strain curve of the materials, and I–III zones cover the elastic, elastic–plastic, and plastic deformation, respectively. Since only the elastic modulus and hardness are extracted from the indentation tests, several assumptions are made for setting material properties in modeling.

1) Yield strength is assumed as $\sigma_y = H/2.8$ [28], ultimate strength $\sigma_u = 1.1 \times \sigma_y$.
2) Tangent modulus during elastic–plastic deformation (region II in Fig. 6) is: $E_t = 5\% \times E$ [28].
3) Poisson's ratio: $\nu = 0.21$, which is the average of Au and CNT.

In the model, the tangent modulus is defined to consider the strain hardening of material, which is not included in most of the contact models. Simulations were carried out with tangent modulus varying from 0 to $10\% \times E$, which are the extreme case for most materials [28]; the difference in force–displacement results was less than 8% for 0.25-mN load; also for most practical material, the tangent modulus is less than 5% [28]. In this paper, $5\% \times E$ was used as tangent modulus for all elastic–plastic material property settings.

As the CNT present supercompressible behavior [15], the CNT forest under layer is considered to deform

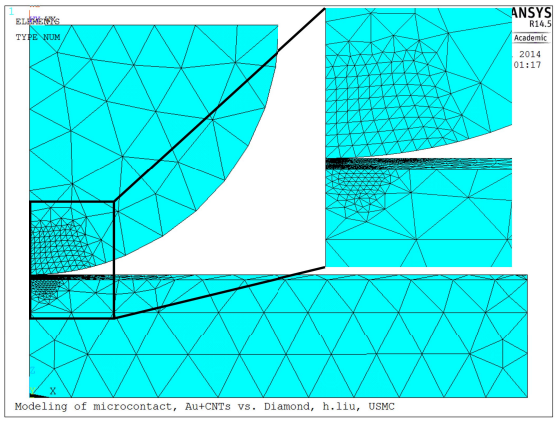

Fig. 7. FE mesh of the model with quarter sized geometry.

elastically only. Poisson's ratio of CNT forest is set as 0, as in [16] and [29]. Poisson's ratio of the top layer is set as 0.21, which is the average of Au and CNT. Though the value of Poisson's ratio was not certain, it was found that it had a weak influence on the mechanical behavior [24], [30]. In addition, previous simulations [19] showed that with the value of Poisson's ratio for the top layer changed from 0 to 0.42, the relative difference for the displacement was less than 4%.

B. Description of Finite Element Model

A FE contact model was used to compare with the nanoindentation test, it includes a diamond hemisphere of 200-μm radius, making contact with a gold-coated CNT composite. The seed and catalyst layers are not included in the modeling. Only a quarter of the hemisphere and substrate is modeled to reduce the computational time (Fig. 7). The Si substrate is modeled as a block with length = width = 800 μm and a thickness of 275 μm. It has been validated that using a larger size for the composite (L, $W > 800$ μm) does not alter the results. Material properties for diamond are elastic modulus $E = 1140$ GPa and Poisson's ratio $\nu = 0.07$ [31].

The FE simulations were performed with ANSYS 14.5. The meshing in contact models is the same as in [32], both deformable bodies are modeled using 3-D tetrahedral solid element SOLID187, which has special features of plasticity, stress stiffening, large deflection, and large strain capabilities. 3-D surface-to-surface contact element CONTA174 and target element TARGE174 are used to mesh the contact surfaces of substrate and hemisphere, respectively. These elements are selected to consider large deflection and nonlinear behavior of contact. The meshing near the contact region is refined to capture the contact accurately, whereas meshing of the rest of volume is coarse, as shown in Fig. 7.

As boundary conditions, the bottom surface of the lower volume is fixed. For all nodes of the top surface of the hemisphere, the degree of freedom UZ is coupled so that they have the same displacement in the z-direction only, and the uniform pressure is applied vertically on the top surface of the hemisphere. A loading–unloading cycle is applied, with an increment/decrement of 0.025 mN, i.e., for a load of 0.25 mN,

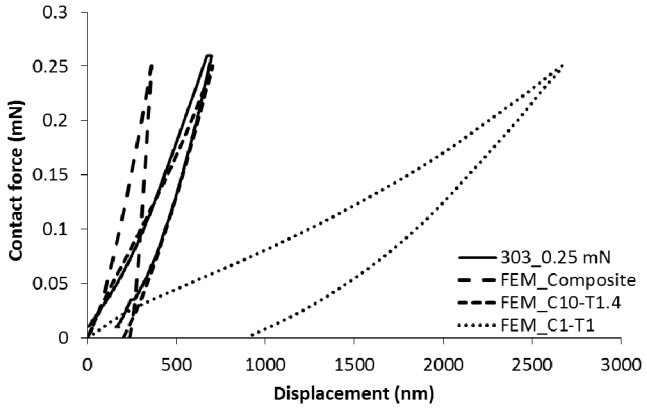

Fig. 8. Comparison between indentation test and FE models for the composite: 300-nm Au/30-μm CNT at 0.25 mN.

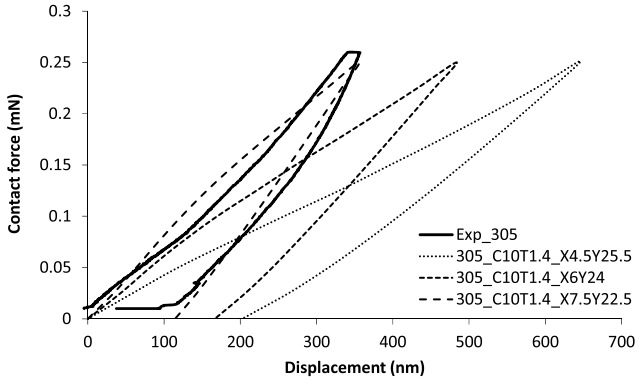

Fig. 9. Comparison between indentation test and FE models with different thicknesses of the top layer for the composite: 500-nm Au/30-μm CNT at 0.25 mN.

it is 10 steps for loading and 10 steps for unloading. The nodes on the symmetric surface cannot move along the normal axis of the symmetric surface, i.e., the displacement of the nodes on surface $X = 0$ is restricted as $UX = 0$, likewise, the displacement of the nodes on surface $Y = 0$ is restricted as $UY = 0$. Simulations were carried out to prove that the model with quarter sized geometry is able to provide good results.

The augmented Lagrange method is used to seek contact in the simulations, and the large deformation is included during the calculation.

IV. Results and Discussion

A. Summary of Previous Results

The initial simulations are shown in Fig. 8, for the composite 300-nm Au/30-μm CNT [19]. The simulation results are for Model I (labeled as FEM_Composite) and Model II with original material settings, [II(a)] in Table II (labeled as FEM_C1-T1).

Three criteria are used to compare the simulations with the experimental data:

1) the trend of the loading and unloading curves;
2) the stiffness at unloading, (used to calculate the elastic modulus), also called the contact stiffness S;
3) maximum displacement $h_{\max}$, residual deformation after unloading h_{res}, and the ratio of $h_{\text{res}}/h_{\max}$. Due to the high elasticity of CNT forest, the unloading curves show different features from metals.

The experimental curves in all figures are the averaged data, with anomalies removed. As creep was not considered in the modeling, the creep deformation was manually subtracted from the experimental unloading curves, to compare the simulated results with the nanoindentation data. The manual offset did not influence the contact stiffness, but reduced the deformation during unloading.

The ratio of $h_{\text{res}}/h_{\max}$ with Model I is 0.66, which is much larger than 0.22 in experiments, whereas the ratio is 0.34 with Model II; this suggests that Model II is a better approach. Simulations were performed to determine the simulation results matching best the test data by adjusting factors of material properties in Model II [19], and it was found that the material setting C10-T1.4 matched the experimental results, where T1.4 means both elastic modulus and hardness of the top layer is multiplied by 1.4, and C10 implies that the elastic modulus of the under layer is multiplied by 10, see Table II, Model II(b) and II(e), respectively. With Model I, the ratio of $h_{\text{res}}/h_{\max}$ was always much larger than that of the experimental data, so modeling the Au/CNT as a single material could not accurately predict the mechanical behavior of Au/CNT. Model II is therefore the preferred approach.

TABLE IV

Simulation Results for Composite 500-nm Au/30-μm CNT With Different Layer Thickness Settings, Compared With the Experimental Results, With a Load Force of 0.25 mN

Models/Exp X=Top layer (μm) Y= Under Layer (μm)	$h_{\max}$ (nm)	h_{res} (nm)	h_{res} / $h_{\max}$	S (N/m)
305_X4.5Y25.5	646	204	0.316	665
305_X6Y24	484	167	0.345	860
305_X7.5Y22.5	356	115	0.323	1097
305_Exp	340	100	0.294	1551

B. Sensitivity of the Model to the Top Layer Thickness (x)

To investigate the effect of the thickness of the top layer (x) on contact behavior of samples, simulations were carried out with different x for the composite 500-nm Au/30-μm CNT, as shown in Fig. 9. The (x) range is

$$x = 6 \pm 1.5\ \mu\text{m}.$$

The simulated values of criteria (h_{res}, $h_{\max}$, $h_{\text{res}}/h_{\max}$ and S) are listed in Table IV, compared with the experimental results. The contact stiffness is calculated from a linear fit of the upper 30% of the unloading curve [21]. It is shown that the thicknesses of the layers have an expected influence on the force–displacement curves, and on the contact stiffness and maximum deformation (Table IV). It has been shown that the thickness of under layer has little influence on the force–displacement curves (not shown in this paper). It is clear that the thickness of the top layer has an important role in the contact behavior of the composite.

The degree of variety is comparable with the variation of nanoindentation tests (Fig. 3), using the setting C10-T1.4 [II(b) and II(e) in Table II] for the composite.

C. Effective Elastic Modulus Calculation

Simulations showed that substrate Si has little influence on the contact behavior of Au/CNT composite, so the influence of Si substrate can be ignored in the calculation of material properties. For a bilayered structure, the determination of effective Young's modulus from the nanoindentation tests depends on the thickness of layers and indenter depth [24], [26], [30], [31], especially for thin films. When the indenter depth is above 0.2–0.3 times of the film thickness, the influence of the under layer must be considered [26].

For a thin film bilayered structure, there are several formulas to calculate the effective Young's modulus [24], [30], [33]–[36]. These are summarized in (4)–(8), where f and s refer to the film and substrate, respectively, and here represent the top and under layers. t is the thickness of the thin film, and α is a parameter, which can be determined empirically. h_c is the contact depth, a_c is the square root of the projected area [30], and a is the mean radius of contact area [35]. E^* is the reduced elastic modulus, and is calculated by $E/(1-\nu^2)$.

$$\frac{1}{E_r} = \frac{1-\nu_i^2}{E_i} + \frac{1-\nu_f^2}{E_f}\left(1-e^{-\alpha t/h_c}\right) + \frac{1-\nu_s^2}{E_s}\left(e^{-\alpha t/h_c}\right) \tag{4}$$

$$\frac{1}{E_r} = \frac{1-\nu_i^2}{E_i} + \frac{1-\nu_f^2}{E_f}\left(1-e^{-\alpha t/a_c}\right) + \frac{1-\nu_s^2}{E_s}\left(e^{-\alpha t/a_c}\right) \tag{5}$$

$$\frac{E^*-E_s^*}{E_f^*-E_s^*} = \Phi_{\text{Gao}} \tag{6}$$

$$\Phi_{\text{Gao}} = \frac{2}{\pi}\arctan\left(\frac{t}{a}\right) + \frac{1}{2\pi(1-2\nu)} \times \left[\begin{array}{l}(1-2\nu)\left(\frac{t}{a}\right)\ln\left(1+\left(\frac{t}{a}\right)^2\right) \\ -\frac{\left(\frac{t}{a}\right)}{1+\left(\frac{t}{a}\right)^2}\end{array}\right] \tag{7}$$

$$\nu = \nu_s + (\nu_f - \nu_s) \times \frac{1}{\pi} \times \left(2\arctan\left(\frac{t}{a}\right) + \frac{t}{a}\times\ln\left(\frac{1+\left(\frac{t}{a}\right)^2}{\left(\frac{t}{a}\right)^2}\right)\right). \tag{8}$$

For a spherical indentation, h_c can be evaluated by [22]

$$h_c = \frac{h_{\max} + h_{\text{res}}}{2}. \tag{9}$$

With the nanoindentation test results, h_c can be calculated with (9), and a_c or a can be calculated with the measured hardness. Furthermore, if the thickness of the top layer is known, there are two unknown parameters E_f and E_s in functions (4)–(6) which can be determined with least square method or optimization method [35]. As parameter α in (4) and (5) depends on the indenter shape and indenter depth [24] and there is no values available for spherical tip, (6) is used in this paper. Equation (6) is based on the results with a cylindrical punch, and is used here as an approximation.

TABLE V
ELASTIC MODULUS CALCULATION FOR THE TOP AND UNDER LAYERS WITH A BILAYERED STRUCTURE THEORY

Composite Au (nm)/ CNT (μm)	FE Modeling [19] E_f (MPa)	E_s (MPa)	Using equation (6) E_f (MPa)	E_s (MPa)
300/30	1242.44	7.26	583.32	0
500/30	1242.44	7.26	1477.56	19.5
800/30	1242.44	7.26	1269.80	0
300/80	887.455	0.726	11.30	0.3

The calculation using (6) was performed for samples modeled in [19], and the results are listed in Table V. It was found that for a composite with 30-μm CNT, the calculated elastic moduli for the top layer E_f are the same order as the values in FEM; however, the values for the under layer E_s are not informative. The values have been set to be nonnegative values, and it was shown that 0 was the best values from calculation for some composites, but it cannot be set as a real material property in modeling. For layer configuration 300-nm Au/80-μm CNT, the calculated values are very different from the values in FEM. It is probably due to the different indenter tip shapes [cylindrical punch in (6) versus hemispherical tip here], and underlying error becomes more significant when the ratio of a/t becomes larger, reaching to 12.3 in this paper, and beyond the range investigated in [24], [30], and [33]–[36], which is up to 4 only. In addition, the elastic moduli of the top and under layers are very different, which adds difficulty to the reliable use of the functions [35]. In addition to this, there is an inherent variability due to the nature of nanotubes, exhibited in the force–displacement curves, as shown in Fig. 3.

Other functions are unable to provide more informative results, so the determination of the elastic modulus of two layers with functions (4)–(8) are shown to be inappropriate in this paper, therefore adjusting factors are used to simulate the experimental results.

D. Results for Samples With Different Thickness Configurations

In [19], it was assumed that for samples with same height CNT, the material properties of two layers are fixed but the layer thicknesses varied depending on the nominal thickness of the gold layer (Table I). The simulations showed a good match for samples with 30-μm CNT under this assumption. For the Au/CNT composite, the top layer is gold penetrating into CNT, so it is further assumed that the material properties of the top layer are the same regardless of layer configurations. It was shown that the material properties T1.4 [II(b) in Table II] provide the simulation results matching with the experimental data for samples with 30-μm CNT (Fig. 8). Simulations were then performed with these two assumptions for samples with 50- and 80-μm CNT.

For samples with 50-μm CNT, the elastic modulus of the under layer should be less than the samples with

TABLE VI
SIMULATION RESULTS FOR COMPOSITE 300-nm Au/50-μm CNT WITH DIFFERENT MATERIAL PROPERTIES SETTINGS, COMPARED WITH THE EXPERIMENTAL RESULTS, APPLIED LOAD 0.25 mN

Models/Exp	h_{max} (nm)	h_{res} (nm)	h_{res} / h_{max}	S (N/m)
503_C3-T1.4	481.67	1668.23	0.289	268
503_C5-T1.4	338.69	1230.16	0.275	349
503_C7-T1.4	267.73	999.76	0.268	416
503_Exp	280	1003	0.279	487

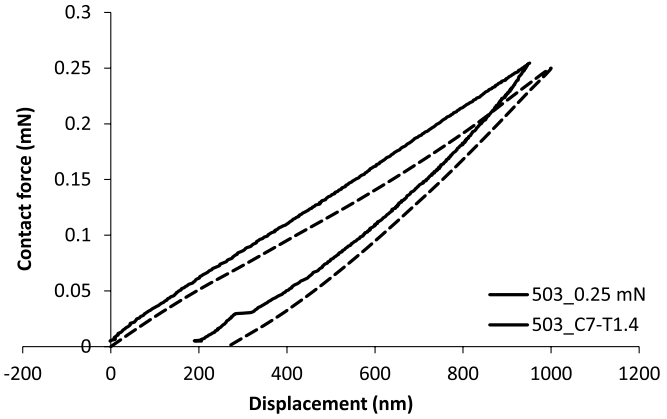

Fig. 10. Comparison between indentation test and FE bilayered model for the composite: 300-nm Au/50-μm CNT at 0.25 mN.

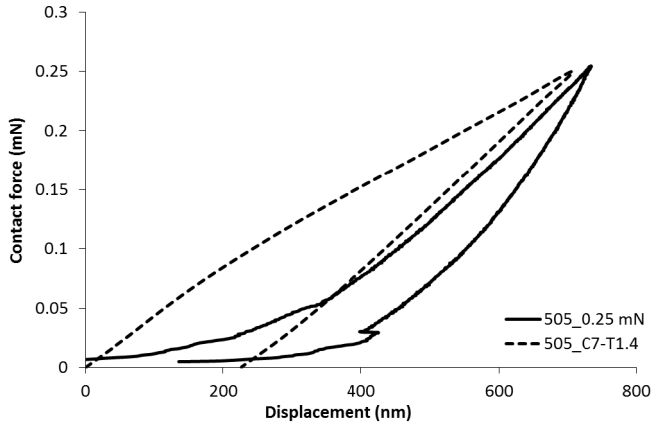

Fig. 11. Comparison between indentation test and FE bilayered model for the composite: 500-nm Au/50-μm CNT at 0.25 mN.

30-μm CNT [16], [20]. Simulations with an adjusting factor of 3, 5, and 7 for the under layer were performed, and the simulation results of h_{res}, h_{max}, h_{res}/h_{max} and contact stiffness S are listed in Table VI. As expected, with the factor increased from 3 to 7, the maximum and residual deformation reduced and the contact stiffness increased. Comparing the criteria in Table VI, simulations with factor 7 matched the best with the experimental results, as shown in Fig. 10.

Material settings C7-1.4 were then used in modeling for composites of 500- and 800-nm gold coated on a 50-μm CNT, and the results are plotted in Figs. 11 and 12, respectively. Though the loading curves showed much stiffer slope,

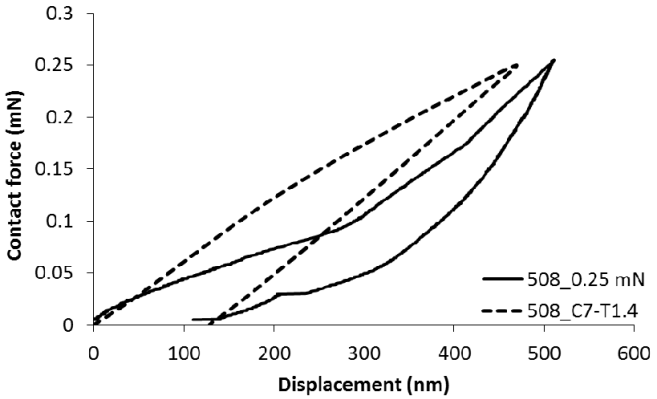

Fig. 12. Comparison between indentation test and FE bilayered model for the composite: 800-nm Au/50-μm CNT at 0.25 mN.

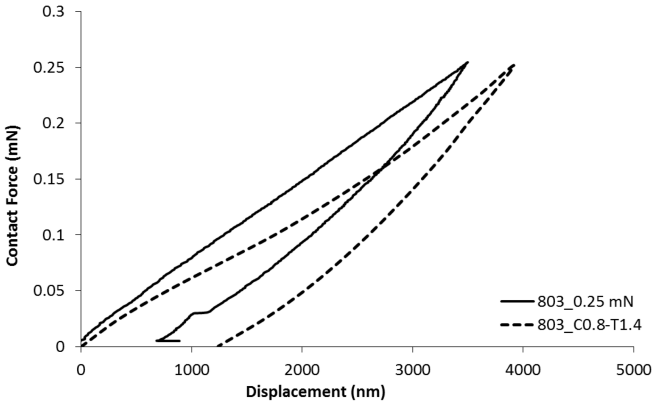

Fig. 13. Comparison between indentation test and FE bilayered model for the composite: 300-nm Au/80-μm CNT at 0.25 mN.

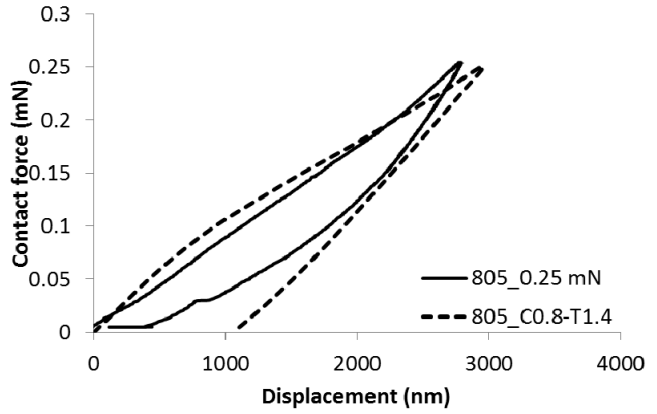

Fig. 14. Comparison between indentation test and FE bilayered model for the composite: 500-nm Au/80-μm CNT at 0.25 mN.

the values of h_{res}, h_{max}, and h_{res}/h_{max}, and the contact stiffness S matched with the experimental results. Looking into the individual nanoindentation tests (Fig. 3), some curves exhibit a plateau at the beginning of loading process, which is probably due to the nonuniform of CNT forest.

For samples with 80-μm CNT, it was shown that an adjusting factor of 0.8 for the under layer compared well with the experimental results, as shown in Figs. 13–15. It should be noted that for the composite with 800-nm coated gold,

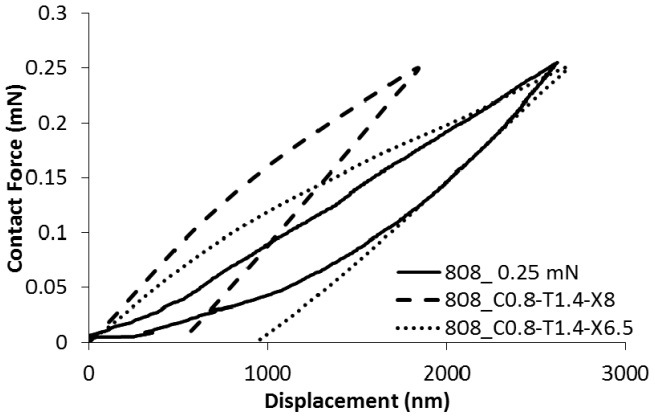

Fig. 15. Comparison between indentation test and FE bilayered models for the composite: 800-nm Au/80-μm CNT at 0.25 mN.

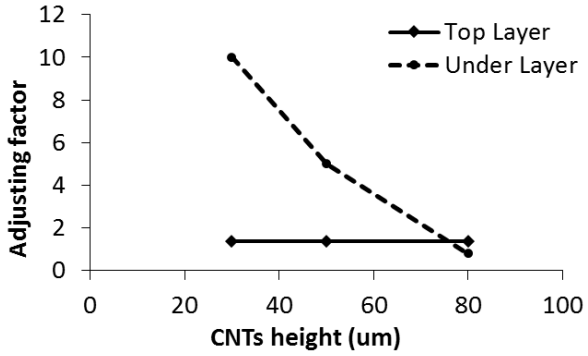

Fig. 16. Adjusting factors for material property settings in FE bilayered modeling.

the thickness of the top layer is better to set as 6.5 μm to match with the experimental data rather than the default value of 8 μm (Fig. 15).

The adjusting factors of material properties for the top and under layers are plotted in Fig. 16 as a function of CNT heights. It is shown that the elastic modulus of the under layer decreases with CNT height, this matches the results demonstrated in [16] and [20], whereas the material properties of the top layer are kept the same.

V. Conclusion

This paper has shown that the FEA approach to modeling these complex Au/CNT composite surfaces yields the results that can be used to allow the optimization of the surfaces.

The nanoindentation data used as the starting point for the model, have shown that the Au/CNT composite surface has an irregular behavior, as reflected in the repeated indentation tests on the same sample. For modeling, an averaged response has been used.

The averaged experimental data have been modeled by determining the contact stiffness and hardness values based on the extreme limits of the experiment, to try to capture the properties of the two layers in the modeling, where the top layer is defined as a mixed elastic–plastic material, and the under layer as a pure CNT. This approach has then been extended by adjusting these extreme values to match the nanoindentation data. The resulting model has been defined by maintaining the material properties of the top layer at a constant 1.4$\times$ the extreme upper value, and by adjusting the material properties of the under and much softer CNT layer.

References

[1] R. A. Coutu, Jr., J. R. Reid, R. Cortez, R. E. Strawser, and P. E. Kladitis, "Microswitches with sputtered Au, AuPd, Au-on-AuPt, and AuPtCu alloy electric contacts," *IEEE Trans. Compon. Packag. Technol.*, vol. 29, no. 2, pp. 341–349, Jun. 2006.

[2] F. Ke, J. Miao, and J. Oberhammer, "A ruthenium-based multimetal-contact RF MEMS switch with a corrugated diaphragm," *J. Microelectromech. Syst.*, vol. 17, no. 6, pp. 1447–1459, Dec. 2008.

[3] A. Broue *et al.*, "Multi-physical characterization of micro-contact materials for MEMS switches," in *Proc. 56th IEEE Holm Conf. Elect. Contacts*, Charleston, SC, USA, Oct. 2010, pp. 1–10.

[4] B. F. Toler, R. A. Coutu, Jr., and J. W. McBride, "A review of micro-contact physics for microelectromechanical systems (MEMS) metal contact switches," *J. Micromech. Microeng.*, vol. 23, no. 10, p. 103001, Oct. 2013.

[5] J. W. McBride, E. M. Yunus, and S. M. Spearing, "Improving the contact resistance at low force using gold coated carbon nanotube surfaces," *Eur. Phys. J. Appl. Phys.*, vol. 50, no. 1, pp. 12904-1–12904-6, Apr. 2010.

[6] E. M. Yunus, J. W. McBride, and S. M. Spearing, "The relationship between contact resistance and contact force on Au-coated carbon nanotube surfaces under low force conditions," *IEEE Trans. Compon. Packag. Technol.*, vol. 32, no. 3, pp. 650–657, Sep. 2009.

[7] E. M. Yunus, S. M. Spearing, and J. W. McBride, "Investigation of gold sputter coated vertically aligned multi-walled carbon nanotubes for RF MEMS contact surfaces," in *Proc. Mater. Res. Soc. Symp.*, Warrendale, PA, USA, 2008, pp. 233–238.

[8] J. W. McBride, C. Chianrabutra, L. Jiang, and S. H. Pu, "The contact resistance performance of gold coated carbon-nanotube surfaces under low current switching," in *Proc. 12th IS-EMD*, Chiba, Japan, 2012, pp. 1–8.

[9] J. W. McBride, S. M. Spearing, L. Jiang, and C. Chianrabutra, "Gold coated carbon-nanotube surfaces as low force electrical contacts for MEMS devices: Part II, fine transfer mechanisms," in *Proc. 57th IEEE Holm Conf. Elect. Contacts*, Minneapolis, MN, USA, Sep. 2011, pp. 1–6.

[10] C. Chianrabutra, L. Jiang, A. P. Lewis, and J. W. McBride, "Evaluating the influence of current on the wear processes of Au/Cr-Au/MWCNT switching surfaces," in *Proc. 59th IEEE Holm Conf. Elect. Contacts*, Newport, RI, USA, Sep. 2013, pp. 1–6.

[11] H. J. Qi *et al.*, "Determination of mechanical properties of carbon nanotubes and vertically aligned carbon nanotube forests using nanoindentation," *J. Mech. Phys. Solids*, vol. 51, nos. 11–12, pp. 2213–2237, Nov. 2003.

[12] B. I. Yakobson and P. Avouris, "Mechanical properties of carbon nanotubes," in *Carbon Nanotubes*, M. S. Dresselhaus, G. Dresselhaus, and P. Avouris, Eds. Berlin, Germany: Springer-Verlag, 2001, pp. 287–327.

[13] R. S. Ruoff, D. Qian, and W. K. Liu, "Mechanical properties of carbon nanotubes: Theoretical predictions and experimental measurements," *Comptes Rendus Phys.*, vol. 4, no. 9, pp. 993–1008, Nov. 2003.

[14] N. J. Ginga, W. Chen, and S. K. Sitaraman, "Waviness reduces effective modulus of carbon nanotube forests by several orders of magnitude," *Carbon*, vol. 66, pp. 57–66, Jan. 2014.

[15] A. Cao, P. L. Dickrell, W. G. Sawyer, M. N. Ghasemi-Nejhad, and P. M. Ajayan, "Super-compressible foamlike carbon nanotube films," *Science*, vol. 310, no. 5752, pp. 1307–1310, Nov. 2005.

[16] Y. Gao, T. Kodama, Y. Won, S. Dogbe, L. Pan, and K. E. Goodson, "Impact of nanotube density and alignment on the elastic modulus near the top and base surfaces of aligned multi-walled carbon nanotube films," *Carbon*, vol. 50, no. 10, pp. 3789–3798, Aug. 2012.

[17] O. Yaglioglu, R. Martens, A. Cao, and A. H. Slocum, "Compliant carbon nanotube-metal contact structures," in *Proc. 57th IEEE Holm Conf. Elect. Contacts*, Minneapolis, MN, USA, Sep. 2011, pp. 1–5.

[18] M. P. Down, R. Cook, L. Jiang, and J. W. McBride, "Mechanical characterisation and optimisation of carbon nanotube composite surfaces for electrical contact," in *Proc. 27th ICEC*, Dresden, Germany, Jun. 2014, pp. 1–6.

[19] H. Liu, M. P. Down, J. W. McBride, S. H. Pu, and L. Jiang, "Mechanical characterization of a Au coated carbon nanotube multi-layered structure," in *Proc. 60th IEEE Holm Conf. Elect. Contacts*, New Orleans, LA, USA, Oct. 2014, pp. 1–8.
[20] K. Eom *et al.*, "Controllable viscoelastic behavior of vertically aligned carbon nanotube arrays," *Carbon*, vol. 65, pp. 305–314, Dec. 2013.
[21] W. C. Oliver and G. M. Pharr, "An improved technique for determining hardness and elastic modulus using load and displacement sensing indentation experiments," *J. Mater. Res.*, vol. 7, no. 6, pp. 1564–1583, Jan. 1992.
[22] W. C. Oliver and G. M. Pharr, "Measurement of hardness and elastic modulus by instrumented indentation: Advances in understanding and refinements to methodology," *J. Mater. Res.*, vol. 19, no. 1, pp. 3–20, Jan. 2004.
[23] *Spherical and Rounded Cone Nano Indenters*. [Online]. Available: http://www.microstartech.com/, accessed Mar. 24, 2014.
[24] R. B. King, "Elastic analysis of some punch problems for a layered medium," *Int. J. Solids Struct.*, vol. 23, no. 12, pp. 1657–1664, 1987.
[25] F. T. Fisher, R. D. Bradshaw, and L. C. Brinson, "Effects of nanotube waviness on the modulus of nanotube-reinforced polymers," *Appl. Phys. Lett.*, vol. 80, no. 24, pp. 4647–4649, Jun. 2002.
[26] W. Peng and B. Bhushan, "A numerical three-dimensional model for the contact of layered elastic/plastic solids with rough surfaces by a variational principle," *J. Tribol.*, vol. 123, no. 2, pp. 330–342, Apr. 2001.
[27] Y. Won *et al.*, "Mechanical characterization of aligned multi-walled carbon nanotube films using microfabricated resonators," *Carbon*, vol. 50, no. 2, pp. 347–355, Feb. 2012.
[28] L. Kogut and I. Etsion, "Elastic-plastic contact analysis of a sphere and a rigid flat," *J. Appl. Mech.*, vol. 69, pp. 657–662, Sep. 2002.
[29] M. R. Maschmann, Q. Zhang, F. Du, L. Dai, and J. Baur, "Length dependent foam-like mechanical response of axially indented vertically oriented carbon nanotube arrays," *Carbon*, vol. 49, no. 2, pp. 386–397, Feb. 2011.
[30] A. K. Bhattacharya and W. D. Nix, "Analysis of elastic and plastic deformation associated with indentation testing of thin films on substrates," *Int. J. Solids Struct.*, vol. 24, no. 12, pp. 1287–1298, 1988.
[31] R. Saha and W. D. Nix, "Effects of the substrate on the determination of thin film mechanical properties by nanoindentation," *Acta Mater.*, vol. 50, no. 1, pp. 23–38, Jan. 2002.
[32] H. Liu, D. Leray, S. Colin, P. Pons, and A. Broué, "Finite element based surface roughness study for ohmic contact of microswitches," in *Proc. 58th IEEE Holm Conf. Elect. Contacts*, Portland, OR, USA, Sep. 2012, pp. 1–10.
[33] M. F. Doerner and W. D. Nix, "A method for interpreting the data from depth-sensing indentation instruments," *J. Mater. Res.*, vol. 1, no. 4, pp. 601–609, Jul./Aug. 1986.
[34] H. Gao, C.-H. Chiu, and J. Lee, "Elastic contact versus indentation modeling of multi-layered materials," *Int. J. Solids Struct.*, vol. 29, no. 20, pp. 2471–2492, 1992.
[35] J. Menčík, D. Munz, E. Quandt, E. R. Weppelmann, and M. V. Swain, "Determination of elastic modulus of thin layers using nanoindentation," *J. Mater. Res.*, vol. 12, no. 9, pp. 2475–2484, Sep. 1997.
[36] J. M. Antunes, J. V. Fernandes, N. A. Sakharova, M. C. Oliveira, and L. F. Menezes, "On the determination of the Young's modulus of thin films using indentation tests," *Int. J. Solids Struct.*, vol. 44, nos. 25–26, pp. 8313–8334, Dec. 2007.

Hong Liu received the B.Sc. degree in mechanical engineering from Shandong University, Jinan, China, in 2006, the M.Sc. degree in mechanical engineering from the South China University of Technology, Guangzhou, China, in 2009, and the Ph.D. degree in mechanical engineering and material mechanics from INSA Toulouse, Toulouse, France, in 2013.

She is currently a Research Fellow with the University of Southampton–Malaysia Campus, Johor Bahru, Malaysia. Her current research interests include microelectromechanical systems switches, carbon nanotubes composites, contact mechanics, and tribology.

Dr. Liu is also the Project Leader of the Ministry of Education Malaysia Grant: Contact Mechanics of Gold Coated Carbon Nanotube Microswitches.

John W. McBride (SM'11) was the Associate Dean of Research with the Faculty of Engineering and the Environment from 2010 to 2011, and the Chair of the Electro-Mechanical Research Group from 1995 to 2010. He is currently the CEO of the University of Southampton–Malaysia Campus, Johor Bahru, Malaysia, and a member of the Electro-mechanical Research Group with the University of Southampton, Southampton, U.K. He is an Expert in electrical contact physics and surface characterization. He has authored over 200 papers, and holds three patents.

Prof. McBride was a recipient of the IEEE Holm Scientific Achievement Award in 2006, an international award for recognizing outstanding scientists and engineers in the field of electrical contacts and related technologies. In 2008, he was the Team Leader for the award of the international James A. Lindner Prize for research on the Sound Archive Project. He is an Associate Editor of the IEEE TRANSACTIONS ON COMPONENTS, PACKAGING, AND MANUFACTURING TECHNOLOGY.

Michael Peter Down received the M.Phys. degree in physics from the University of York, Heslington, U.K., in 2012. He is currently pursuing the Ph.D. degree with the University of Southampton, Southampton, U.K., and the University of Southampton—Malaysian Campus, Johor Bahru, Malaysia.

He is currently a Post-Graduate Researcher. His current research interests include microelectromechanical systems switches, carbon nanotubes composites, contact mechanics, and tribology.

Mr. Down's work is supported by the Innovative Electronics and Manufacturing Research Council and the Engineering and Physical Sciences Research Council.

Suan Hui Pu (M'11) received the M.Eng. degree in mechanical engineering and the Ph.D. degree in electrical and electronic engineering from Imperial College London, London, U.K., in 2006 and 2010, respectively.

He was a Product Engineer with Infineon Technologies (Kulim) Sdn. Bhd., Kulim, Malaysia, from 2010 to 2012, where he was involved in product yield enhancement for a bipolar-CMOS–DMOS process technology. He is currently an Assistant Professor with the University of Southampton–Malaysia Campus, Johor Bahru, Malaysia, and a Visiting Academician with the Nano Research Group, School of Electronics and Computer Science, University of Southampton, Southampton, U.K. He has authored over 16 peer-reviewed papers in international journals and conferences. His current research interests include microelectromechanical systems/nanoelectromechanical systems sensors and actuators, graphene, nanocrystalline graphite, and wearable technology.

Dr. Pu currently serves as a Technical Committee Member of the IEEE Electronics Packaging Technology Conference, and a Reviewer of the IEEE JOURNAL OF MICROELECTROMECHANICAL SYSTEMS.